Facile and controllable synthesis of monodisperse gold nanoparticle bipyramid for electrochemical dopamine sensor

Lavita Nuraviana Rizalputri[1,2*], Isa Anshori[2,3*], Murni Handayani[4], Gilang Gumilar[2,5], Ni Luh Wulan Septiani[4,5], Yeni Wahyuni Hartati[6,7], Muhammad Sjahrul Annas[8], Agnes Purwidyantri[10], Briliant Adhi Prabowo[10,11*], Brian Yuliarto[2,5*]

[1]Department of Nanotechnology, Graduate School, Bandung Institute of Technology, Bandung, Indonesia

[2]Research Center for Nanoscience and Nanotechnology (RCNN), Bandung Institute of Technology, Bandung, Indonesia

[3]Department of Biomedical Engineering, Bandung Institute of Technology, Bandung, Indonesia

[4]Research Center for Advanced Materials, National Research and Innovation Agency (BRIN), Tangerang Selatan, Indonesia

[5]Advanced Functional Materials Laboratory, Engineering Physics Department, Bandung Institute of Technology, Bandung, Indonesia

[6]Department of Chemistry, Faculty of Mathematics and Natural Sciences, Universitas Padjadjaran, Sumedang, Indonesia

[7]Research Center of Molecular Biotechnology and Bioinformatics, Universitas Padjadjaran, Bandung, Indonesia

[8]Department of Mechanical Engineering, Universitas Trisakti, Jakarta, Indonesia

[9]School of Chemistry and Chemical Engineering, Queen's University Belfast, Belfast, United Kingdom

[10]Research Center for Electronics, National Research and Innovation Agency (BRIN), Bandung, Indonesia

[11]International Iberian Nanotechnology Laboratory, Braga, Portugal

*Corresponding authors: lavita.nuraviana@gmail.com, isaa@staff.stei.itb.ac.id, briliant.prabowo@inl.int, brian@tf.itb.ac.id

Abstract

We demonstrated potential features of gold nanoparticle bipyramid (AuNB) for an electrochemical biosensor. The facile synthesis method and controllable shape and size of the AuNB are achieved through the optimization of cetyltrimethylammonium chloride (CTAC) surfactant over citric acid ratio determining the control of typically spherical Au seed size and its transition into a penta-twinned crystal structure. We observe that the optimized ratio of CTAC and citric acid (CA) facilitates flocculation control in which Au seeds with size as tiny as ~14.8 nm could be attained and finally transformed into AuNB structures with an average length of ~55 nm with high reproducibility. To improve the electrochemical sensing performance of a screen-printed carbon electrode (SPCE), surface modification with AuNB via distinctive linking procedures effectively enhanced the electroactive surface area by 40%. Carried out for the detection of dopamine (DA), a neurotransmitter frequently linked to the risk of Parkinson's, Alzheimer's, and Huntington's diseases, the AuNB decorated-carbon electrode shows outstanding electrocatalytic activity that improves sensing performance, including high sensitivity, low detection limit, wide dynamic range,

high selectivity against different analytes, such as ascorbic acid (AA), uric acid (UA) and urea, and excellent reproducibility.

1. Introduction

Gold nanoparticle (AuNP) is one of the most widely used metal materials as sensing membranes due to its high biological compatibility, large surface-to-volume ratio, high stability, non-toxicity, strong electromagnetic field, and fast electron transfer[1–3]. Either bottom-up or top-down AuNPs-based sensor has raised great attention on enhancing the sensitivity of biochemical sensing for various targets and sensing mechanisms [4–9]. Specifically, in electrochemical biosensors signal amplification, the electroactive surface area plays a pivotal role in determining effective sensitivity and specificity due to the increasing binding sites toward the analysis of particular analytes[10]. The carbon-based electrodes modified with AuNP were proposed for several applications, such as, DNA hybridization[8], Microcystin-LR[11], glucose[12], hydrogen peroxide[4,13,14], and other potential applications[15]. The commercially available screen-printed electrode has been a remarkable alternative to conventional glassy carbon electrode (GCE) that requires accompanying instruments, a large solution volume, and a time-consuming and tedious cleaning process [16].The size, shape, and aspect ratio of nanoparticles to modify the electrode are key parameters to improving the sensing capability due to their electrocatalytic activity and optical properties[18]. Ren et al. discovered that sensitivity relied on the surface crystallographic orientations and shape, with greater sensitivity validated with the largest number of Au (111) facets on the surface for the nanoparticles [17]. In another report, Au nanospikes and dendrites were used, formed by electrodeposition with adjustment of directing agent and plating duration. Alternatively, Zeng et al. reported that the catalytic activity of Au nanocages is greater than that of nanoboxes and nanoparticles toward the reduction of p-nitrophenol by $NaBH_4$ [18]. These studies prove that nanoparticle's dimensional, morphological and topological characteristics affect the electrochemical response, particularly sensitivity.

Gold nanoparticle bipyramid (AuNB) offers distinguished dimension and shape monodispersity among myriads of engineered nanostructures. Moreover, it possesses broadly explorable properties for electroactive surface area enhancement owing to its three-dimensional double-tipsy structure for easier interaction of bioanalytes at the sensing interface. The application of gold bipyramids for optical biosensors has been well studied. However, the profound investigation of its potencies for electrochemical enhancement is not yet widely exploited and is an exciting topic in the advancement of the point of care (PoC) unit. Cheng et al. reported a study in modified GCE with gold nanobipyramid/multi-walled carbon nanotube hybrids (AuNB/MWCNTs) to detect dopamine in the presence of ascorbic acid and uric acid with a detection limit of 15 nM [19]. From the side of AuNB synthesis, the seed-mediated growth method has been widely used because it can produce a uniform nano bipyramid. However, controlling the crystal characteristics of the seeds, which ultimately dictates the crystallinity and form of the resultant nanoparticles, remains crucial [20,21].

Many researchers suggested cetyltrimethylammonium bromide (CTAB) as a stabilization agent for monodispersed gold nanoparticle synthesis [22–24]. The main reason for the CTAB preferences is the presence of strong halide ions of Br^- from CTAB on the gold surface that offers better control of the nanoparticle's growth and stability [24]. Nevertheless, for a particular application, such as biosensing elements, the strong binding of these ions leads to a challenging surface functionalization process. These trade-off features can be compromised for particular and functional applications of the gold nanoparticles. It was reported that CTAC offers milder accumulations of Cl^- halide ions on the gold surface compared to the CTAB [20,23,25,26]. Sanchez et al. disclosed a protocol for preparing Au seeds, whereas, with the presence of CTAC and citric acid, $HAuCl_4$ was reduced by $NaBH_4$ [21]. Chateau et al., reported the thermal aging of CTAC gold seeds in acidic media to synthesize gold bipyramid with good reproducibility and reasonable yield[27]. Sánchez-Iglesias et al., 2007 verified the effectivity of this approach to yield highly stable penta-twinned seeds from the monocrystalline Au [21]. Although CTAC and citric acid attach to the metal surface, the citrate ions are known to trigger the creation of twin defects [28]. However, there are few studies about the effect of citrate ion concentration on the Au seed's properties to craft gold bipyramid structures in aqueous-based synthesis.

Neurotransmitters are biological substances that transport a signal from a neuron across the synapse to a target cell, making them necessary for the central and peripheral nervous systems to operate [29,30]. Dopamine (DA) is an essential neurotransmitter associated with numerous central nervous system processes such as motor regulation, reward, reinforcement [29,31], movement, cognition, and addictive behaviors [32]. DA system dysfunction has been linked to various nervous system illnesses, such as Alzheimer's, Parkinson's, and Huntington's, if the person has a lower dopamine concentration than commonly [31,32]. On the contrary, a high dopamine level implies cardiotoxicity, resulting in rapid heart rate, hypertension, heart failure, and drug addiction [33,34]. For that reason, monitoring dopamine levels is critical for the early diagnosis and treatment of those conditions. Conventional analytical methods used to measure dopamine include liquid chromatography [35–38], mass spectroscopy [37,38], and capillary electrophoresis [39,40] are robust and have become the golden standard for accuracy, yet, it is costly due to sophisticated equipment and laborious procedure [29].

In terms of neurotransmitter detection using biosensors, electrochemical biosensor offers superior suitability. Electroactive neurotransmitters, such as dopamine (DA) and serotonin (5-HT) are biomolecular models that can be directly detected electrochemically due their potentials that could be recorded at the specific potential window of metal surfaces [41,42]. There are achievable routes toward unambiguous screening of neurotransmitter biomolecules electrochemically. The common approaches are electrode modification via the deposition of nanomaterials as a redox mediator, surface modification with active groups to reinforce charge transfer, and the deposition of high surface area nanostructures to improve the electrode's sensitivity. Particularly for DA detection, significant challenges may arise from the low amount of dopamine concentration in physiological samples (0–0.25 nM in blood and 0.3–3 μM in urine) [43] and selectivity against other interfering analytes, such as ascorbic acid (AA) and uric acid (UA) [44,45]. Various

modifications on the surface of the electrode were conducted to improve the electrocatalytic characteristics leading to better sensitivity and specificity, such as using metal [46–49] and metal oxide nanomaterial [44,50], carbon nanomaterial [51,52], polymer [53,54], and composites [19,55,56]. Chelly et al., presented an electrochemical sensor for *Rhanterium suaveolens* plant extract using AuNP modified electrodes with an LoD around 0.2 µM by the presence of interference substance ascorbic acid (AA) and uric acid (UA) for dopamine detection [57], indicating the powerful impact of AuNP as working electrode (WE) modifier.

In this research, we propose a comprehensive study of the effect of citrate ions from citric acid (CA) on tuning the gold seed size toward gold bipyramid nanostructure synthesis. We found out that the most suitable ratio of CTAC and CA could efficiently downscale the Au seed, favoring controllable AuNB's size and shape for modification of electrochemistry electrodes. SPCE surface modification with synthesized AuNB is optimized via several linking protocols. The AuNB-modified electrode is applied as an electrochemical sensor for dopamine detection. Outcomes show that the fabricated biosensor enables a wide dynamic range detection with considerably high sensitivity, a low detection limit of 37 nM, high selectivity against interfering analytes, and exceptional reproducibility.

2. Materials and Methods

2.1. Materials

Cetyltrimethylammonium chloride (CTAC), citric acid (CA) ($C_6H_8O_7$), gold (III) chloride trihydrate ($HAuCl_4 \cdot 3H_2O$), sodium borohydride ($NaBH_4$), silver nitrate ($AgNO_3$), hydrochloric acid (HCl), L-ascorbic acid ($C_6H_8O_6$), dopamine hydrochloride ($C_8H_{12}ClNO_2$), Nafion, sulfuric acid (H_2SO_4), phosphate buffer saline (PBS), 1,4-dithiothreitol (DTT), potassium ferricyanide (III) ($K_3[Fe(CN)_6]$), uric acid ($C_5H_4N_4O_3$) and urea (CH_4N_2O) was purchased from Sigma-Aldrich. These chemicals were analytical grade and used without further purification. All aqueous solution was performed using distilled water.

2.2. Methods

2.2.1. Synthesis and characterization of AuNB

We used a two-step seed-mediated growth process to synthesize AuNB (Figure S1 in supplementary material) [21,24]. First, the initial gold seed and the growth of AuNB were thermally treated toward a high-yield AuNB [21]. Firstly, the seed solution was prepared using a vial. A 4 mL of 0.5 M CTAC solution, 0.9 mL of 0.01 M $HAuCl_4$, and 2 mL of CA with three different concentrations to obtain CTAC:CA ratios of 20:1, 20:2 and 20:3 were used. Subsequently, the solutions were mixed in distilled water with a total volume of 40 mL. A 1 mL of freshly prepared 0.06 M $NaBH_4$ was added to the mixture. All mixing processes were carried out under vigorous stirring. Next, the seed solution was heated in an oil bath at 80°C for 90 minutes until the solution turned brownish red. Accordingly, the AuNB was synthesized, started by adding 9 mL of 0.5 M CTAC, 2.2 mL of 0.01 M HAuCl4, 0.4 mL of 0.01 M $AgNO_3$, 0.9 mL of 1 M HCl, 0.4 mL of 0.1 M of ascorbic acid, and 4 mL of Au seed solution into distilled water to a total

volume of 50 mL. The addition was carried out rapidly under vigorous stirring. The mixture was then stored at 30°C overnight and undisturbed until the AuNB obtained was dark purple. For morphological analysis, a transmission electron microscope (TEM) HITACHI HT7700 (Hitachi, Ltd., Tokyo, Japan) was employed. The nanoPartica SZ-100V2 particle size analyzer (Horiba, Ltd., Kyoto, Japan) was used to measure particle size and distribution. The Evolution 220 UV-Visible Spectrophotometer (Thermo Fisher Scientific, Cambridge, England) was utilized to monitor the absorbance peak of the particles.

2.2.2. *Electrode modification with AuNB and electrochemical characterization*

The modification with AuNB was done on a screen-printed electrode (SCPE) with a size of 25.4 mm × 7 mm × 0.625 mm used as a working electrode (WE). Prior to modification, the activation step was done by dropping 50 mL of 0.5 M H_2SO_4 onto the SPCE. The activation took place by three cycles of cyclic voltammetry from 0.9 V to 1.5 V with a scan rate of 100 mV/s. This step was mandatory for removing organic cross-linking from carbon and enhancing surface roughness and functionality to improve electrocatalytic performance [58]. The WE electrode surface was then modified using drop-casting of AuNB. Initially, the AuNB solution was prepared, and the excess surfactant from 1 mL AuNB stock was removed by centrifugation up to 12.300 g for 15 minutes and then redispersed in 1 mL distilled water. To ensure the uniform coverage of AuNB onto the electrode surface, several approaches were tested. In the first method, 1 µL of the prepared AuNB solution was dropped directly onto the electrode and dried at room temperature for about 30 minutes, followed by the dropping of 1 µL Nafion 5% after the AuNB was dry. Another method employed the drop of 1 µL of 0.01 M DTT that stood to dry at room temperature, followed by the dropping of 1 µL of AuNB solution. For AuNB amount optimization, the solution was dropped repeatedly (one to five times). The washing protocols were always done with distilled water. Electrochemical characteristics of the sensor material were performed using Zimmer Peacock Ana Pot 4X – EIS – ZP1000080 electrochemical workstation (Zimmer Peacock Ltd, Warwickshire, England) with a three-electrode system setup, including hyper value screen-printed electrode (HVSPE) from Zimmer Peacock with the carbon working electrode (WE), silver (Ag) counter electrode (CE), and silver/silver chloride (Ag/AgCl) for the reference electrode (RE). For cyclic voltammetry (CV) measurement, the 50 mV/s scan rate and three cycle parameters in a solution containing ferri/ferrocyanide ions were applied.

2.2.3. *Application of AuNB-modified electrode for dopamine sensor*

Chronoamperommetry was used in dopamine detection using the AuNB-modified electrode. Initially, we performed curve stabilization for 200 s using PBS 0.01M (pH 7.4). This protocol was followed by the measurement of a series of dopamine concentrations ranging from 0.1–100 µM for 100 s per concentration. The current signal was extracted from the average data point measured for 50-100 s. For selectivity detection, the AuNB-modified electrode was essentially exposed to a 1 M dopamine with the presence of interfering analytes, such as AA, UA, and urea, during the measurement. In the reproducibility study, we tested five individual sensors to detect 1 mM DA

and recorded their chronoamperometric signals. The general workflow of dopamine detection using the AuNB-modified electrode in this study is shown in Figure 1.
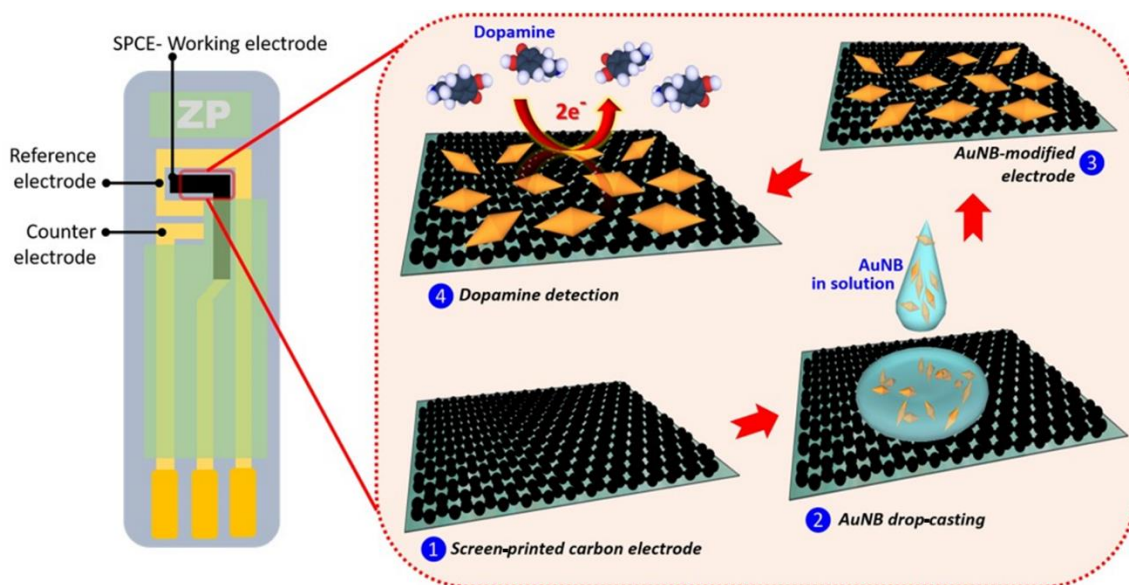
Figure 1. Schematic illustration of dopamine detection using the AuNB-modified electrode.

2.2.4. Statistical analysis

For the statistical analysis results, all the standard deviations in the calibration plots were taken from triplicate measurements on a sensor under an identical experimental protocol. The linear fitting function from Origin 9 software (OriginLab, Northampton, MA, USA) is applied. From the linear regression curve, the limit of detection (LoD) and Limit of Quantification (LoQ) can also be determined using the equation [59], with σ being a standard deviation and s is the slope of the linear regression curve.

$$LoD = \frac{3.3\sigma}{s} \qquad \text{(Eq. 1)}$$

$$LoQ = \frac{10\sigma}{s} \qquad \text{(Eq. 2)}$$

3. Result and Discussion

3.1. Characterization of Au seed and gold nanoparticle bipyramid

Au seed preparation is the critical factor for successful penta-twinned crystal formation for AuNB production. Changes in crystal structure and morphology can be adjusted by adjusting experimental parameters such as temperature, CA concentration, or the presence of other organic additives [21]. In this study, we applied constant CTAC concentration, 0.5 M. While the CTAC:CA ratios of 20:1, 20:2, and 20:3 were represented by 0.05 M, 0.1 M, and 0.15 M citric acid concentrations, respectively. Figures 2(a) and (b) display the prepared Au seed's consistencies in absorbance and purple-red color intensity for all the ratios tested at around 520 nm wavelength. It also implies that all the Au seed solutions are formed in a spherical structure, typically resulting

in a clear single peak with a homogeneous shape and localized surface plasmon resonance (LSPR) properties around this wavelength [60]. It occurred due to the reduction of the precursor $AuCl_4^-$ to Au^0 by $NaBH_4$ (as a strong reducing agent) and was stabilized by CTAC, forming the spherical gold [61].

It is important to note that CTAC acts as a stabilizing agent for Au nanoseeds due to the presence of halide ions (Cl^- ions). Meanwhile, CA serves as both a reducing and stabilizing agent. The stabilizing effect of CA results from the presence of citric ions, which also fall within the halide groups. However, the more powerful metal-binding properties of Cl^- from CTAC typically surpass the stabilizing activity of CA. Hence, the reducing capability of CA is now playing the dominant role in controlling the chemical and kinetic interactions, allowing a change in the crystallinity and size of the gold seeds.

As a reducing agent for gold seeds formation, the chemical reaction involving CA can be described as follows:

$$2HAuCl_4 + 3C_6H_8O_7 \text{ (citric acid)} \rightarrow 2Au + 3C_5H_6O_5 + 8HCl + 3CO_2$$
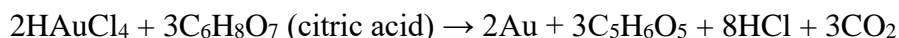
The higher concentration of CA leads to the Au monomers' stronger surface potential, which enhances the Au monomers' interaction to form the gold seeds. In addition, the higher concentration of CA (or lower ratio of CTAC:CA) leads to the formation of larger gold seeds, as demonstrated in Figure 2(c). On the other hand, a lower CA concentration (or higher CTAC:CA ratio) is preferable to construct smaller gold nanoseeds. Furthermore, the lower CA concentration (or higher CTAC:CA ratio) also leads to the higher density of halide ions of Cl^- from CTAC because of the low competitiveness between Cl^- and citrate ions. The high affinity of halide ions on the gold surface was described in detail by Meena et al.[23]. The Cl^- halide ions protect and stabilize the gold seeds' surface during the reduction process of the precursor $AuCl_4^-$ to Au^0 by $NaBH_4$. Consequently, the higher ratio of CTAC:CA resulting a smaller size of gold nanoparticles (spherical shapes) with good stability. Next, for AuNB growth, identical precursors were used for the three initial gold nanoparticle production. The precursor solution contains: 9 mL of 0.5 M CTAC, 2.2 mL of 0.01 M $HAuCl_4$, 0.4 mL of 0.01 M $AgNO_3$, 0.9 mL of 1 M HCl, 0.4 mL of 0.1 M of AA. In this process, the anisotropic growth of gold nanoseed forms AuNB shape. The anisotropic growth can be explained, due to the different energy binding of the halide ions on the different crystalline of gold, especially strongest in the Au (111) orientation compared to the other orientations[23,24]. This mechanism leads to rapid nanoparticle growth in Au (110) orientation and slower growth in Au (111) direction; therefore, the AuNB can be formed.

The absorbance peak for AuNB from Au seed prepared with 0.05 M, 0.10 M, and 0.15 M is at 527.0, 526.0, and 527.8 nm, respectively (Figure 2(d)). In addition, the absorbance behavior shows that AuNB from seed solution prepared with the lowest concentration of citrate exhibits the highest longitudinal peak, corresponding to a higher AuNB yield shown by vertically localized surface plasmon resonance (LSPR) properties [21,62,63]. Figure 2(e) concomitantly verifies the absorbance characterization of the synthesized AuNB by the significant changes of the red/purple color of the solution toward dark brownish as the citrate solution is reduced. Such color alterations imply the formation of bipyramids with various aspect ratios and shapes, which means a lower amount of spheres [21].
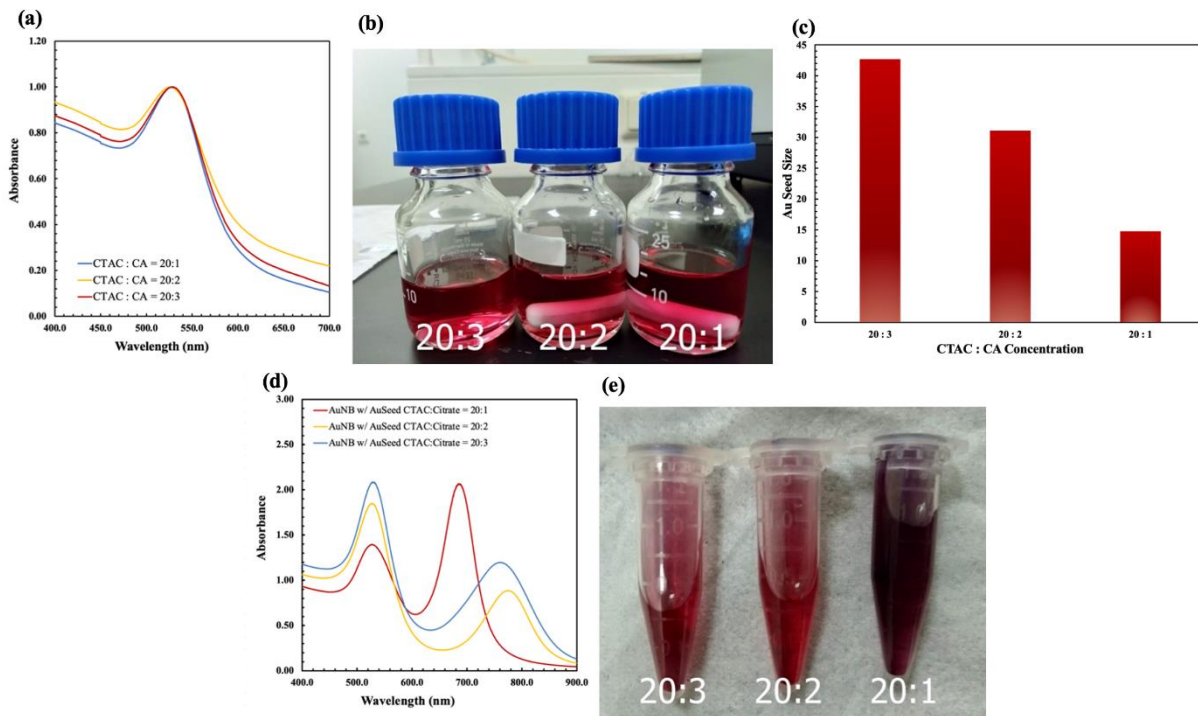
Figure 2. (a) absorbance characteristics of Au seed, (b) photograph of Au seed solution, (c) Au seed size (d) absorbance characteristics of AuNB, and (e) photograph of the color difference of AuNB solution from Au seed prepared with varying CTAC:CA ratio.

Morphological characteristics of the synthesized AuNB portrayed by TEM affirm the optical properties mentioned above. Figures 3(a) and (b) reveal that with 0.15 M citrate, most of the particles remain spherical, with some pseudo-spherical and nanorod to dumb-bell structures with an average length of ~17.7 nm. With lower citrate concentration down to 0.1 M, as seen in Figures 3(c) and (d), we observed that some particles turn into a rice-like structure where slightly sharp tips at both corners start to appear with an average length of ~54.7 nm. Subsequently, with the lowest citrate concentration at 0.05 M (CTAC:CA ratio 20:1), most of the seeds successfully transformed into bipyramid structures with much sharper tips than those produced with higher citrate concentrations, with preserved penta-twinned crystallinity and an average length of ~54.8 nm (Figure 3(e) and (f)). A complete series of particle size analysis of the produced AuNB is presented in Figure S4. Our findings attest to the importance of adjusting surfactant and acid ratio for more controllable monodisperse seed into AuNB structures since excessive surfactant concentration may trigger specific issues, including highly viscous solution, solubility problems, and uncontrollable flocculation and transformation from spherical micellar seeds to rod-like or worm-like structure [24,64].
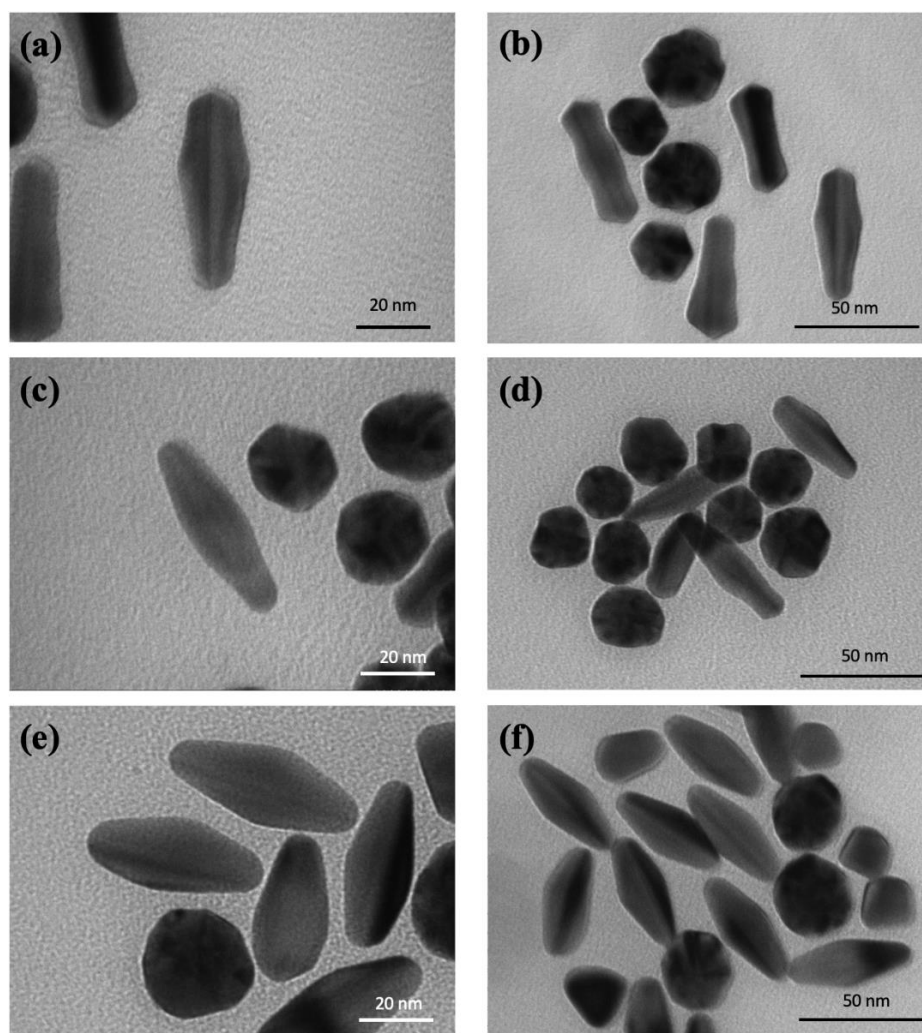
Figure 3. TEM images of the AuNBs synthesized by various ratios of CTAC:CA at (a and b) 20:3, (c and d) 20:2, and (e and f) 20:1, in different magnifications.

3.2 Electrochemical characterization of AuNB-modified electrode

The drop-casting method is opted for due to its low cost and simplicity compared to other techniques, such as ink mixing [65]. To determine the presence of AuNB, 0.5 M H_2SO_4 was used to evaluate the characteristic of polycrystalline Au, represented by the appearance of a reduction peak in acidic conditions [19]. This peak is caused by the reduction of Au oxides during the positive potential scan [17,19,66]. To provide firm immobilization of AuNB onto the SPCE, a binder is needed. In this research, Nafion and DTT were used. Nafion is one of the binders commonly used for the drop-casting method. Meanwhile, DTT with disulfide compound binds the AuNB through an Au-thiol bond [67]. As seen in Figure 4(a), there is no reduction peak for bare SPCE, while a reduction peak at 0.7 V was recorded for AuNB-direct drop cast onto the electrode surface. Surface treatments with AuNB-Nafion and DTT-AuNB result in Ip_{red} of 2.14, 1.37, and 2.56 µA, respectively, implying the most effective AuNB immobilization via the DTT linking

agent. Accordingly, the CV measurement for $[Fe(CN)_6]^{3-}/[Fe(CN)_6]^{4-}$ redox reaction was conducted to determine the electrochemical response of the AuNB linking protocols, as seen in Figure 5(b). The redox peak and electroactive surface area in the modified electrode were obtained using Eq. 3 [14,68], where Ip is the peak current (µA), n is the number of electrons, D_R is the diffusion coefficient (cm^2 s^{-1}), C is the analyte concentration (µM), v is the scan rate (V s^{-1}), and A is the electrode electroactive surface area (cm^2). Diffusion coefficient for ferrocyanide is 6.2 x 10^{-6} cm^2 s^{-1} [14].

$$Ip = 2.69 \times 10^5 \, A \, n^{3/2} \, D_R^{1/2} \, C \, v^{1/2} \qquad \text{(Eq. 3)}$$
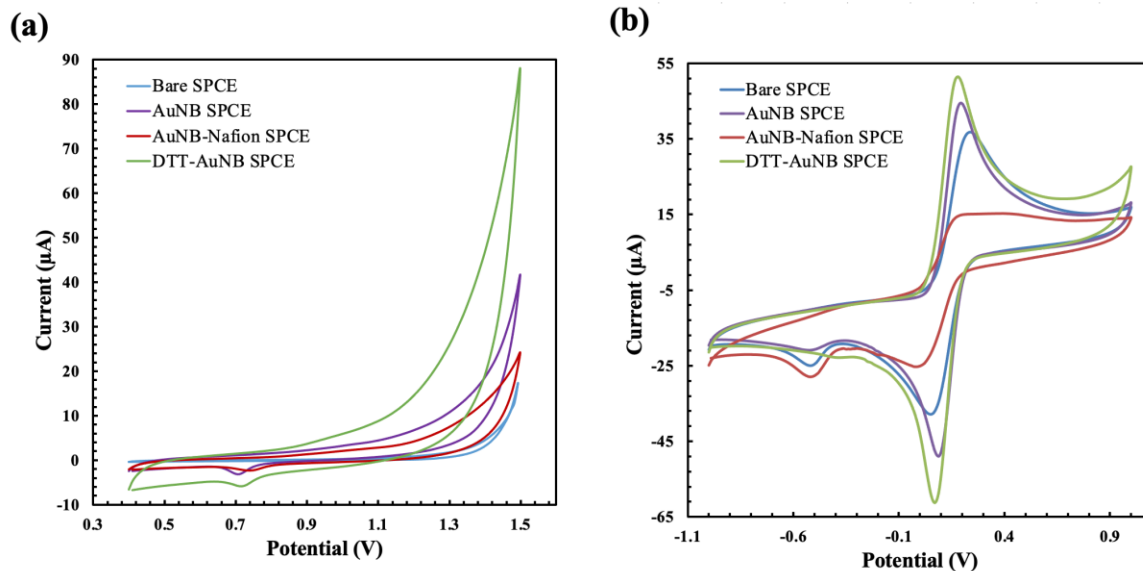
Figure 4. (a) AuNP characterization by CV using 0.5 M H_2SO_4 analyte and (b) using $[Fe(CN)_6]^{3-}$ /$[Fe(CN)_6]^{4-}$ redox probe to determine the effectivity of AuNB immobilization onto the electrode using different linkers.

Table 1 summarizes that the DTT provides effective AuNB immobilization and coverage on the SPCE, shown by a much higher oxidation peak and electroactive surface area than other linking methods. Before using the modified electrode for dopamine detection, we also studied the optimized volume of AuNB for an effective electrochemical response. Tested with 1 to 5 µL of AuNB solution, the cyclic voltammogram presents that an optimum cathodic current peak response at −48.55 µA was achieved with 4 µL of AuNB solution drop-casted onto the SPCE (Figure S2).

In Figure 4(b), the Nafion role as the AuNB binder leads to a significantly drop in the electrochemistry signals. This phenomenon can be explained by the fact that Nafion is a polymer that is highly selective for proton exchanges [69]. This material blocks the electrons, which leads to the very low current peaks of the electrochemistry measurements.

Table 1. Peak current (Ip) and electroactive surface area value from the anodic peak from various surface modifications on SPCE

	Ip (µA)	Electroactive Surface Area (cm^2)
Bare	40.42	0.027
AuNB – Nafion	19.17	0.013
AuNB	49.75	0.033
DTT – AuNB	56.86	0.038

3.3 The electrochemical sensing performance of AuNB-modified electrode for dopamine sensor

The electrochemical response of AuNB-modified electrode for dopamine sensing is initially recorded by CV in the measurement of PBS without and with 1 mM DA. The response against the presence of dopamine substantially results in four peaks corresponding to the redox reactions of dopamine at the sensing interface, as shown in Figure 5(a), while no peaks were observed under the measurement with only PBS. Comparative electrochemical response in Figure 5(b) suggests the higher electrocatalytic performance of AuNB-modified electrode by the increment of 3.64% and 1.21% of anodic and cathodic peak currents, respectively, from the bare state (Table S1), induced by accelerated electron transfer process between the analyte and the surface [70]. Meanwhile, the four electrochemical reactions in DA detection include an anodic (peak I) and cathodic (peak II) peak that form a pair related to dopamine that is oxidized and becomes dopamine o quinone (DQ) reaction (Figure 5(c)). Another pair is a cathodic (peak III) and an anodic (peak IV) peak associated with the cyclization of DQ to form Leukoaminochrome (Figure 5(d)) [71]. The second reaction occurred because the measurement conditions were at a neutral pH (7.4), causing additional cyclization and polymerization reactions. Since this reaction could be minimized at low pH resulting in only the first reaction occurrence [71], we focus on peaks I and II. We also observed a diffusion-controlled mechanism in dopamine sensing by applying the ascending scan rates from 25 to 200 mV/s (Figure S3). The selectivity of the sensor was tested to detect various analytes, namely 1 mM dopamine, 1 mM ascorbic acid (AA), 1 mM uric acid (UA), and 10 mM in 0.01 mM PBS or urea. As seen in Figure 5e, the bare electrode shows low selectivity by the appearance of only one prominent peak at the same potential when exposed to different analytes. In contrast, the AuNB-modified electrode establishes higher selectivity by the appearance of varying peak locations ascribing to the measurement of dopamine, AA, UA, and urea with resulting potentials of -0.3 V and 0.15 V, -0.1 V, 0.27 V, and 0.05 V, respectively.
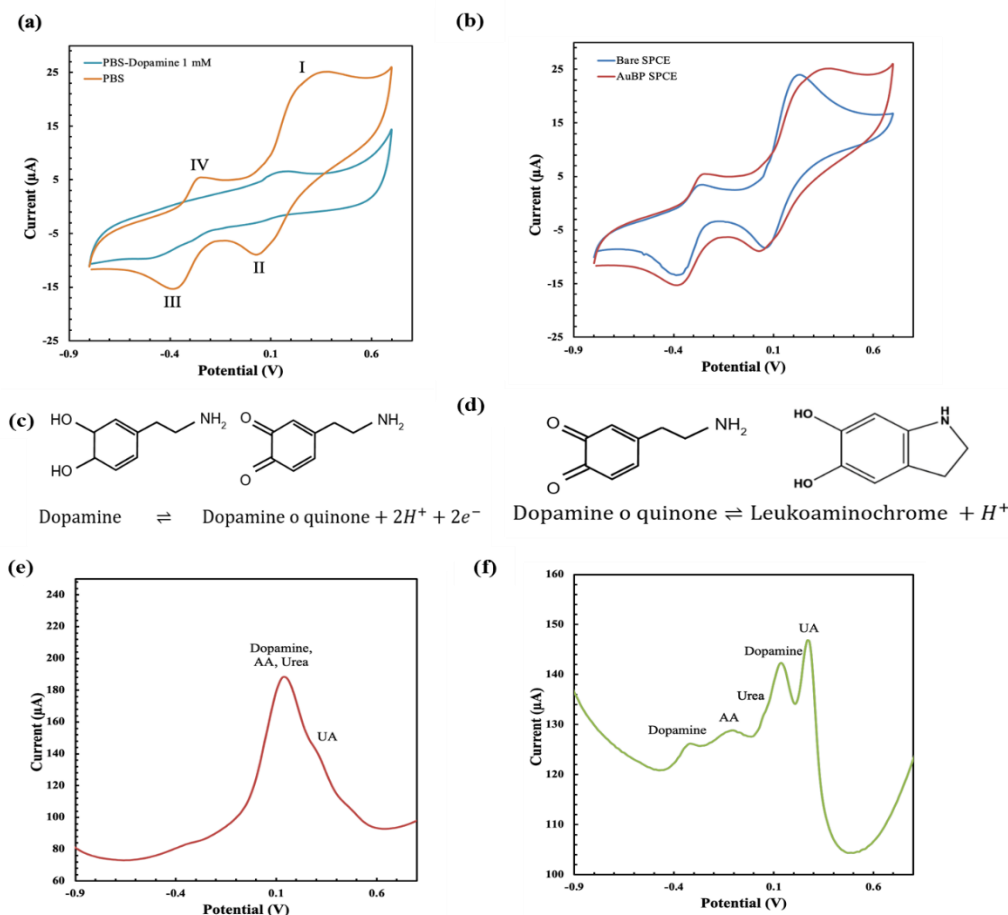
Figure 5 Comparison of cyclic voltammogram in the measurement of (a) PBS without and with dopamine using AuNB-modified electrode, (b) 1 mM dopamine using bare and AuNB-modified electrode, (c) the first, and (d) the second dopamine redox reactions, and selectivity of (e) bare electrode and (f) AuNB-modified electrode in detecting different analytes

The sensitivity of the sensor is evaluated by measuring a series of dopamine concentrations by chronoamperometry. This technique was chosen due to its high sensitivity, resulting in a low limit of detection (LoD) [19]. Figure 6(a) displays a real-time chronoamperogram of the increased dopamine tested. The linear regression curve of dopamine detection in the dynamic range of 0.1 to 100 μM with the correlation coefficient (R^2) of 0.9974 is seen in Figure 6(b). The sensor shows excellent sensitivity of 0.1133 μA μM^{-1} cm^{-2} dopamine, which is significantly higher than several other published reports on electrochemical dopamine sensors [47,57], implying the versatility and efficiency of our developed AuNB-based sensor. Regarding detection limit, from equations 1 and 2, it is calculated that the proposed sensor produces an outstanding LoD of 0.037 μM with accuracy and repeatability represented by LoQ of 0.113 μA. The elicited detection limit falls below the detection range for dopamine in urine (0.3–3 μM), designating the suitability of the sensor in a clinical setting.
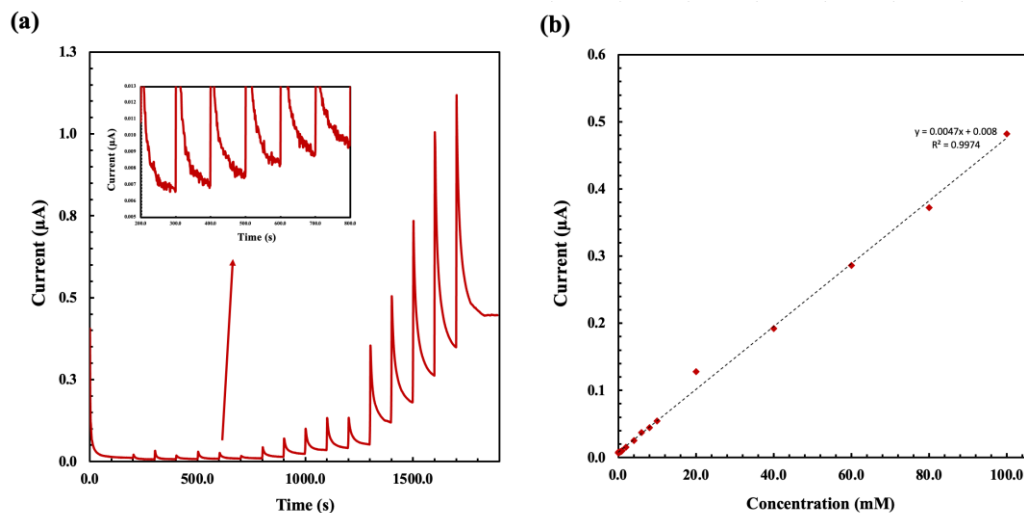
Figure 6. (a) chronoamperometry results and (b) calibration plot of the measurement of dopamine concentrations ranging from 0.1–100 µM.

The reproducibility of the AuNB electrochemical sensor is of great importance for its practical application. Amperometry signals of five different AuNB-modified SPCEs to 1 mM dopamine were monitored under the same conditions. As shown in Figure 7(a), the amperometry measurement shows the stability of the five individual sensors for measuring 1 mM DA with the anodic peak current in CV measurement for each sensor plotted in Figure 7(b). It is calculated that the coefficient of variation from this dataset is less than 3.45% (with a mean of 1.9%), indicating remarkable reproducibility of the AuNB-modified electrode for DA detection. The chronoamperometry method is also used to revalidate the selectivity screening performed earlier with CV. It is shown that the amperometric signals could clearly distinguish the pure DA and other analytes. Being tested with the dopamine mixed with other analytes, the sensor recovers a considerably stable signal as in pure dopamine measurement with slightly lower value that could be the impact of the interfering agents. Nevertheless, this behavior is indicative of the proposed sensor's ability to detect dopamine in complex matrices.

The performance factors comparison with previously published works in dopamine electrochemical sensing devices is compiled in Table 2. These reported works represent an important milestone in the advancement of electrochemical detection of dopamine to date. While in terms of sensitivity and dynamic range, our system is highly comparable with the published results, a significant highlight is a real-time detection, in which our proposed system outperforms most previous research applying various nanomaterials. It is also noteworthy that being compared to AuNP sphere composites with other materials such as MoS_2, reduced Graphene Oxide (rGO) and Graphene (G), our AuNB-modified electrode produces a smaller LoD in detecting dopamine [72–74]. Outstanding LoD and real-time detection offered by our AuNB-modified electrode are significantly necessitated for dopamine detection in clinical settings.
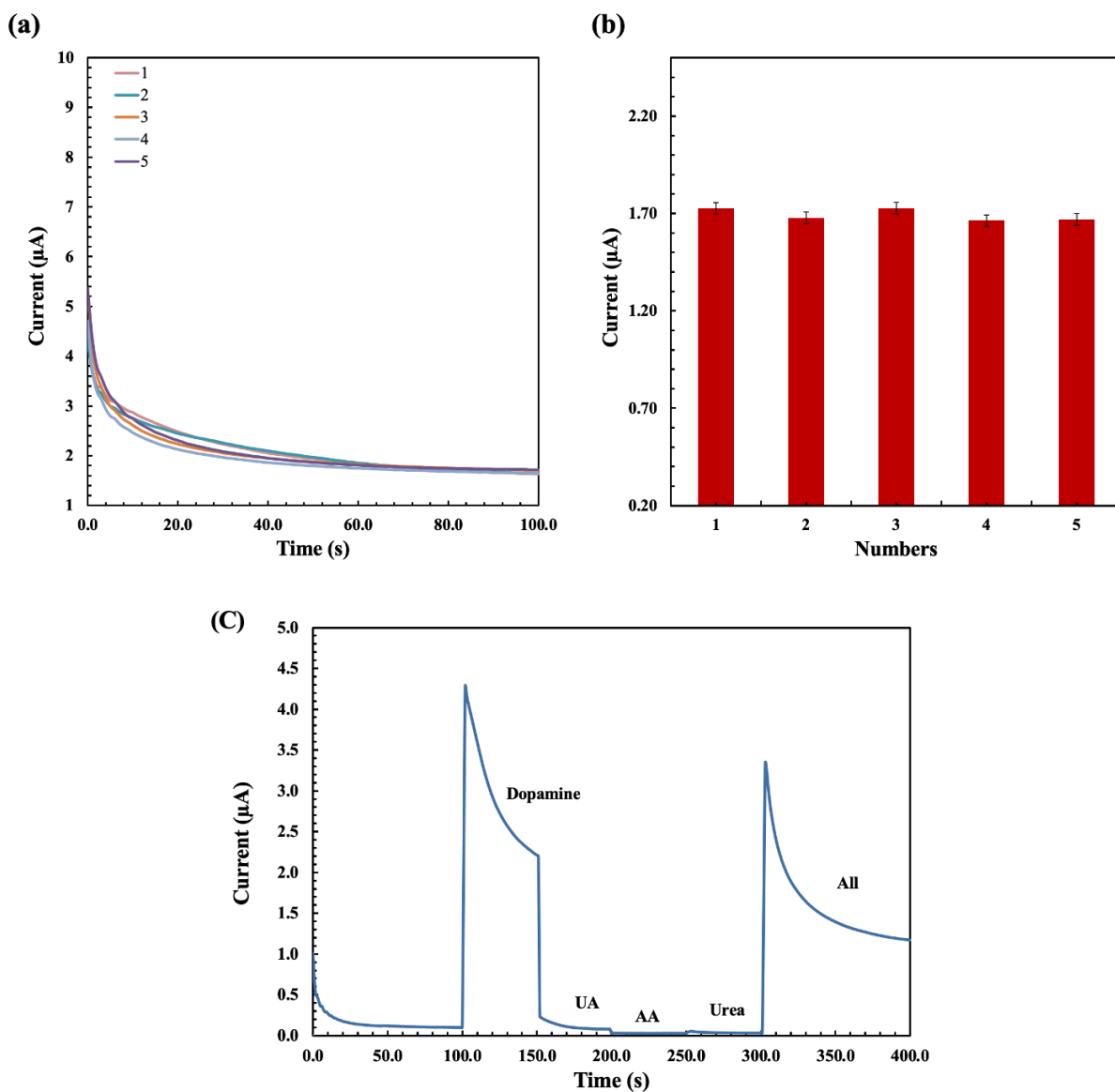
Figure 7. (a) amperometry measurement of five different AuNB-modified electrodes for detecting 1 mM DA in PBS 7.4, (b) Ip of the anodic peak from the CV measurement, and (c) selectivity of the AuNB-modified electrode against pure DA, UA, AA, urea and DA mixed with UA, AA, urea measured with chronoamperometry.

Table 2. A summary of related literatures of electrochemistry sensors for dopamine detection.

Modified Material	Linear Range (µM)	LOD (µM)	Sensitivity (µA µM^{-1} cm^{-2})	Real time	Method / Sensor Used	Ref
AuNP	2–58	0.2	550.4	No	DPV / SPCE	[57]
AuNP	10–600	0.7	0.15	No	DPV / GCE	[47]

MoS$_2$/Au	0.5–300	0.076	n/a	No	DPV / CPE	[72]
rGO/AuNPs	0.1–100	0.095	n/a	No	DPV / GCE	[74]
Au-G	0.08–600	0.05	n/a	Yes	Amperometric / CPE	[73]
AuNBPs/MWCNT	0.05–2700	0.015	n/a	No	Amperometric / GCE	[19]
AuNR@ZIF-8	0.1−50	0.03	n/a	No	CV / GCE	[75]
AuNB	0,1–100	0.037	0.113	Yes	Amperometric / SPCE	This Works

DPV = Differential Pulse Voltammetry

4 Conclusions

We have designed a facile synthesis of gold nanoparticle bipyramid (AuNB) by optimizing surfactant and acid ratio leading to a smaller Au seed for controllable growth into AuNBs with improved catalytic activity. We found that maintaining citrate ions at low concentrations and allowing higher CTAC is pivotal in yielding tinier Au seed and transforming its spherical structure toward penta-twinned crystal of bipyramid Au. Carried out to modify an electrochemical working electrode, the AuNB exhibits remarkable electrochemical properties, such as electroactive surface area enhancement through a simple and low-cost drop-cast method and thiol-binding mechanism, thanks to the handy and commercially available screen-printed carbon electrode that paves an avenue for miniaturization and convenient use of sensors. Being applied as dopamine sensor, the AuNB-modified electrode results in a wide dynamic range detection with considerably outstanding sensitivity, rapid response, low detection limit, high selectivity, and reproducibility. Overall, the proposed AuNB-modified sensor showcases excellent sensing characteristics and high potential in developing electrochemical point-of-care devices.

Author contributions:

Lavita N. Rizalputri: Conceptualization, Methodology, Investigation, Validation, Formal Analysis, Writing-Original Draft. Isa Anshori: Conceptualization, Resources, Formal Analysis, Writing-Original Review & Editing, Supervision. Gilang Gumilar: Methodology, Formal Analysis. Ni Luh Wulan Septiani: Formal Analysis, Writing-Original Review & Editing. Yeni Wahyuni Hartati: Conceptualization. Muhammad Sjahrul Annas: Conceptualization, Resources. Murni Handayani: Conceptualization, Formal Analysis. Agnes Purwidyantri: Validation, Writing-Original Review & Editing. Briliant Adhi Prabowo: Validation, Validation, Writing-Original Review & Editing. Brian Yuliarto: Conceptualization, Resources, Formal Analysis, Supervision. All authors discuss the results, and agree the manuscript final version.

REFERENCE

[1]   Xiao T, Huang J, Wang D, Meng T and Yang X 2020 Au and Au-Based nanomaterials: Synthesis and recent progress in electrochemical sensor applications *Talanta* **206**

[2]   Atta N F, Galal A and El-Said D M 2019 Novel Design of a Layered Electrochemical Dopamine Sensor in Real Samples Based on Gold Nanoparticles/β-Cyclodextrin/Nafion-Modified Gold Electrode *ACS Omega* **4**

[3]   Gupta A K, Hsu C-H H, Chen C-H H, Purwidyantri A, Prabowo B A, Wang J-L L, Tian Y-C C and Lai C-S S 2019 Au-spotted zinc oxide nano-hexagonrods structure for plasmon-photoluminescence sensor *Sensors Actuators B Chem.* **290** 100–9

[4]   Purwidyantri A, Tian Y, Muhammad G, Saputra A and Prabowo B A 2021 Gold Nanoframe Array Electrode for Straightforward Detection of Hydrogen Peroxide *Chemosensors* **9** 37

[5]   Bonyár A, Csarnovics I, Veres M, Himics L, Csik A, Kámán J, Balázs L and Kökényesi S 2018 Investigation of the performance of thermally generated gold nanoislands for LSPR and SERS applications *Sensors Actuators, B Chem.*

[6]   Ma H, Chen Z, Gao X, Liu W and Zhu H 2019 3D hierarchically gold-nanoparticle-decorated porous carbon for high-performance supercapacitors *Sci. Rep.* **9** 17065

[7]   Ahmed S R, Kim J, Tran V T, Suzuki T and Neethirajan S 2017 In situ self-assembly of gold nanoparticles on hydrophilic and hydrophobic substrates for influenza virus-sensing platform *Sci. Rep.* **7** 44495

[8]   Prabowo B A, Purwidyantri A, Liu B, Lai H C and Liu K C 2021 Gold nanoparticle-assisted plasmonic enhancement for DNA detection on a graphene-based portable surface plasmon resonance sensor *Nanotechnology* **32** 095503

[9]   Liu J, Jalali M, Mahshid S and Wachsmann-Hogiu S 2020 Are plasmonic optical biosensors ready for use in point-of-need applications? *Analyst* **145** 364–84

[10]   Hsu C H, Gupta A K, Purwidyantri A, Prabowo B A, Chen C H, Chuang C C, Tian Y C, Lu Y J and Lai C S 2022 Sensing Alzheimer's Disease Utilizing Au Electrode by Controlling Nanorestructuring *Chemosensors* **10**

[11]   Tian M, Wang J, Li C, Wang Z, Liu G, Lv E, Zhao X, Li Z, Cao D, Liu H, Zhang C, Xu S and Man B 2022 Qualitative and quantitative detection of microcystin-LR based on SERS-FET dual-mode biosensor *Biosens. Bioelectron.* **212** 114434

[12]   Viswanathan S, Narayanan T N, Aran K, Fink K D, Paredes J, Ajayan P M, Filipek S, Miszta P, Tekin H C, Inci F, Demirci U, Li P, Bolotin K I, Liepmann D and Renugopalakrishanan V 2015 Graphene-protein field effect biosensors: Glucose sensing *Mater. Today* **18** 513–22

[13]   Patella B, Buscetta M, Di Vincenzo S, Ferraro M, Aiello G, Sunseri C, Pace E, Inguanta R and Cipollina C 2021 Electrochemical sensor based on rGO/Au nanoparticles for monitoring H2O2 released by human macrophages *SENSORS AND ACTUATORS B-CHEMICAL* **327**

[14]   Elewi A S, Al-Shammaree S A W and AL Sammarraie A K M A 2020 Hydrogen peroxide biosensor based on hemoglobin-modified gold nanoparticles–screen printed carbon electrode *Sens. Bio-Sensing Res.* **28**

[15]   Maduraiveeran G, Sasidharan M and Ganesan V 2018 Electrochemical sensor and biosensor platforms based on advanced nanomaterials for biological and biomedical applications *Biosens. Bioelectron.* **103** 113–29

[16]   Ratnam K V, Manjunatha H, Janardan S, Babu Naidu K C and Ramesh S 2020

Nonenzymatic electrochemical sensor based on metal oxide, MO (M= Cu, Ni, Zn, and Fe) nanomaterials for neurotransmitters: An abridged review *Sensors Int.* **1** 100047

[17]   Ren B, Jones L A, Chen M, Oppedisano D K, Qiu D, Ippolito S J and Bhargava S K 2017 The Effect of Electrodeposition Parameters and Morphology on the Performance of Au Nanostructures for the Detection of As (III) *J. Electrochem. Soc.* **164**

[18]   Zeng J, Zhang Q, Chen J and Xia Y 2010 A comparison study of the catalytic properties of Au-based nanocages, nanoboxes, and nanoparticles *Nano Lett.* **10**

[19]   Cheng J, Wang X, Nie T, Yin L, Wang S, Zhao Y, Wu H and Mei H 2020 A novel electrochemical sensing platform for detection of dopamine based on gold nanobipyramid/multi-walled carbon nanotube hybrids *Anal. Bioanal. Chem.* **412** 2433–41

[20]   Chateau D, Liotta A, Vadcard F, Navarro J R G, Chaput F, Lermé J, Lerouge F and Parola S 2015 From gold nanobipyramids to nanojavelins for a precise tuning of the plasmon resonance to the infrared wavelengths: Experimental and theoretical aspects *Nanoscale* **7** 1934–43

[21]   Sánchez-Iglesias A, Winckelmans N, Altantzis T, Bals S, Grzelczak M and Liz-Marzán L M 2017 High-Yield Seeded Growth of Monodisperse Pentatwinned Gold Nanoparticles through Thermally Induced Seed Twinning *J. Am. Chem. Soc.* **139** 107–10

[22]   Liu M and Guyot-Sionnest P 2005 Mechanism of silver(I)-assisted growth of gold nanorods and bipyramids *J. Phys. Chem. B* **109** 22192–200

[23]   Meena S K, Celiksoy S, Schäfer P, Henkel A, Sönnichsen C and Sulpizi M 2016 The role of halide ions in the anisotropic growth of gold nanoparticles: A microscopic, atomistic perspective *Phys. Chem. Chem. Phys.* **18** 13246–54

[24]   Lee J H, Gibson K J, Chen G and Weizmann Y 2015 Bipyramid-templated synthesis of monodisperse anisotropic gold nanocrystals *Nat. Commun.* **6** 7571

[25]   Balbuena Ortega A, Arroyo Carrasco M L, Méndez Otero M M, Gayou V L, Delgado Macuil R, Martínez Gutiérrez H and Iturbe Castillo M D 2014 Nonlocal nonlinear refractive index of gold nanoparticles synthesized by ascorbic acid reduction: Comparison of fitting models *J. Mod. Opt.* **61**

[26]   Weng G, Dong X, Li J and Zhao J 2016 Halide ions can trigger the oxidative etching of gold nanorods with the iodide ions being the most efficient *J. Mater. Sci.* **51** 7678–90

[27]   Chateau D, Desert A, Lerouge F, Landaburu G, Santucci S and Parola S 2019 Beyond the Concentration Limitation in the Synthesis of Nanobipyramids and Other Pentatwinned Gold Nanostructures *ACS Appl. Mater. Interfaces* **11** 39068–76

[28]   Xiong Y, McLellan J M, Yin Y and Xia Y 2007 Synthesis of palladium icosahedra with twinned structure by blocking oxidative etching with citric acid or citrate ions *Angew. Chemie - Int. Ed.* **46** 790–4

[29]   Lakard S, Pavel I A and Lakard B 2021 Electrochemical biosensing of dopamine neurotransmitter: A review *Biosensors* **11**

[30]   Kerage D, Sloan E K, Mattarollo S R and McCombe P A 2019 Interaction of neurotransmitters and neurochemicals with lymphocytes *J. Neuroimmunol.* **332** 99–111

[31]   Juárez Olguín H, Calderón Guzmán D, Hernández García E and Barragán Mejía G 2016 The role of dopamine and its dysfunction as a consequence of oxidative stress *Oxid. Med. Cell. Longev.* **2016**

[32]   Dalirirad S and Steckl A J 2020 Lateral flow assay using aptamer-based sensing for on-site detection of dopamine in urine *Anal. Biochem.* **596** 113637

[33]   Feng P, Chen Y, Zhang L, Qian C G, Xiao X, Han X and Shen Q D 2018 Near-Infrared

Fluorescent Nanoprobes for Revealing the Role of Dopamine in Drug Addiction *ACS Appl. Mater. Interfaces* **10**

[34] Liu W W, Hashim U and Rao Balakrishnan S 2012 *Carbon nanotubes-based electrochemical biosensors*

[35] Wu D, Xie H, Lu H, Li W and Zhang Q 2016 Sensitive determination of norepinephrine, epinephrine, dopamine and 5-hydroxytryptamine by coupling HPLC with [Ag(HIO6)2]5−–luminol chemiluminescence detection *Biomed. Chromatogr.* **30**

[36] Zhao H X, Mu H, Bai Y H, Yu H and Hu Y M 2011 A rapid method for the determination of dopamine in porcine muscle by pre-column derivatization and HPLC with fluorescence detection *J. Pharm. Anal.* **1**

[37] Kim H R, Kim T H, Hong S H and Kim H G 2012 Direct detection of tetrahydrobiopterin (BH4) and dopamine in rat brain using liquid chromatography coupled electrospray tandem mass spectrometry *Biochem. Biophys. Res. Commun.* **419**

[38] Ribeiro R P, Gasparetto J C, De Oliveira Vilhena R, De Francisco T M G, Martins C A F, Cardoso M A and Pontarolo R 2015 Simultaneous determination of levodopa, carbidopa, entacapone, tolcapone, 3-O-methyldopa and dopamine in human plasma by an HPLC-MS/MS method *Bioanalysis* **7**

[39] Roychoudhury A, Francis K A, Patel J, Jha S K and Basu S 2020 A decoupler-free simple paper microchip capillary electrophoresis device for simultaneous detection of dopamine, epinephrine and serotonin *RSC Adv.* **10**

[40] Fang H, Pajski M L, Ross A E and Venton B J 2013 Quantitation of dopamine, serotonin and adenosine content in a tissue punch from a brain slice using capillary electrophoresis with fast-scan cyclic voltammetry detection *Anal. Methods* **5**

[41] Liu N, Xiang X, Fu L, Cao Q, Huang R, Liu H, Han G and Wu L 2021 Regenerative field effect transistor biosensor for in vivo monitoring of dopamine in fish brains *Biosens. Bioelectron.* **188** 113340

[42] Zamani M, Wilhelm T and Furst A L 2022 Perspective—Electrochemical Sensors for Neurotransmitters and Psychiatrics: Steps toward Physiological Mental Health Monitoring *J. Electrochem. Soc.* **169** 47513

[43] Steckl A J and Ray P 2018 Stress Biomarkers in Biological Fluids and Their Point-of-Use Detection. *ACS sensors* **3** 2025–44

[44] Fayemi O E, Adekunle A S, Kumara Swamy B E and Ebenso E E 2018 Electrochemical sensor for the detection of dopamine in real samples using polyaniline/NiO, ZnO, and Fe3O4 nanocomposites on glassy carbon electrode *J. Electroanal. Chem.* **818**

[45] Mahbubur Rahman M and Lee J J 2021 Sensitivity control of dopamine detection by conducting poly(thionine) *Electrochem. commun.* **125**

[46] Qin X, Zhang J, Shao W, Liu X, Zhang X, Chen F, Qin X, Wang L, Luo D and Qiao X 2021 Modification of electrodes with self-assembled, close-packed AuNPs for improved signal reproducibility toward electrochemical detection of dopamine *Electrochem. commun.* **133**

[47] Suresh Kumar P, Megarajan S, Reddy G R K and Anbazhagan V 2018 Facile synthesis of gold nanoparticles using carbon dots for electrochemical detection of neurotransmitter, dopamine in human serum and as a chemocatalyst for nitroaromatic reduction *IET Nanobiotechnology* **12**

[48] Memon R, Memon A A, Nafady A, Sirajuddin, Sherazi S T H, Balouch A, Memon K, Brohi N A and Najeeb A 2021 Electrochemical sensing of dopamine via bio-assisted

synthesized silver nanoparticles *Int. Nano Lett.* **11**

[49] Vidya H, Kumara Swamy B E and Schell M 2016 One step facile synthesis of silver nanoparticles for the simultaneous electrochemical determination of dopamine and ascorbic acid *J. Mol. Liq.* **214** 298–305

[50] Swamy B K, Shiprath K, Venkata Ratnam K, Manjunatha H, Janardan S, Ratnamala A, Chandra Babu Naidu K, Ramesh S and Babu K S 2020 Electrochemical detection of dopamine and tyrosine using metal oxide (MO, M=Cu and Ni) modified graphite electrode: A comparative study *Biointerface Res. Appl. Chem.* **10**

[51] Arumugasamy S K, Govindaraju S and Yun K 2020 Electrochemical sensor for detecting dopamine using graphene quantum dots incorporated with multiwall carbon nanotubes *Appl. Surf. Sci.* **508**

[52] Huang Q, Lin X, Tong L and Tong Q X 2020 Graphene Quantum Dots/Multiwalled Carbon Nanotubes Composite-Based Electrochemical Sensor for Detecting Dopamine Release from Living Cells *ACS Sustain. Chem. Eng.* **8**

[53] Chen X, Wu G, Cai Z, Oyama M and Chen X 2014 Advances in enzyme-free electrochemical sensors for hydrogen peroxide, glucose, and uric acid *Microchim. Acta* **181** 689–705

[54] Ran G, Chen X and Xia Y 2017 Electrochemical detection of serotonin based on a poly(bromocresol green) film and Fe3O4 nanoparticles in a chitosan matrix *RSC Adv.* **7**

[55] Anshori I, Nuraviana Rizalputri L, Rona Althof R, Sean Surjadi S, Harimurti S, Gumilar G, Yuliarto B and Handayani M 2021 Functionalized multi-walled carbon nanotube/silver nanoparticle (f-MWCNT/AgNP) nanocomposites as non-enzymatic electrochemical biosensors for dopamine detection *Nanocomposites* **7**

[56] Anbumannan V, Kumar R T R and Suresh K 2021 Enhanced electrochemical detection of dopamine by graphene oxide/tungsten trioxide nanocomposite *Mater. Sci. Semicond. Process.* **127**

[57] Chelly S, Chelly M, Zribi R, Gdoura R, Bouaziz-Ketata H and Neri G 2021 Electrochemical Detection of Dopamine and Riboflavine on a Screen-Printed Carbon Electrode Modified by AuNPs Derived from Rhanterium suaveolens Plant Extract *ACS Omega* **6**

[58] Wan H, Sun Q, Li H, Sun F, Hu N and Wang P 2015 Screen-printed gold electrode with gold nanoparticles modification for simultaneous electrochemical determination of lead and copper *Sensors Actuators, B Chem.* **209**

[59] Shrivastava A and Gupta V 2011 Methods for the determination of limit of detection and limit of quantitation of the analytical methods *Chronicles Young Sci.* **2** 21

[60] Jeon H Bin, Tsalu P V and Ha J W 2019 Shape Effect on the Refractive Index Sensitivity at Localized Surface Plasmon Resonance Inflection Points of Single Gold Nanocubes with Vertices *Sci. Rep.* **9** 1–8

[61] Agunloye E, Panariello L, Gavriilidis A and Mazzei L 2018 A model for the formation of gold nanoparticles in the citrate synthesis method *Chem. Eng. Sci.* **191**

[62] Zhang H, She Z, Su H, Kerman K and Kraatz H B 2016 Effects of bipyramidal gold nanoparticles and gold nanorods on the detection of immunoglobulins *Analyst* **141**

[63] Geitner N K, Doepke A, Fickenscher M A, Yarrison-Rice J M, Heineman W R, Jackson H E and Smith L M 2011 The morphology and evolution of bipyramidal gold nanoparticles *Nanotechnology* **22**

[64] Park K, Koerner H and Vaia R A 2010 Depletion-induced shape and size selection of

gold nanoparticles *Nano Lett.* **10** 1433–9

[65] Antuña-Jiménez D, González-García M B, Hernández-Santos D and Fanjul-Bolado P 2020 Screen-printed electrodes modified with metal nanoparticles for small molecule sensing *Biosensors* **10**

[66] Alshamaileh E, Saadeh H and Favry V 2013 Modification of Gold surface with gold nanoparticles and cyclohexyl dithiocarbamate as a selective sensor for cysteine *J. Chem.*

[67] Wang B T and Wang Q 2018 Sensitivity-Enhanced Optical Fiber Biosensor Based on Coupling Effect between SPR and LSPR *IEEE Sens. J.* **18** 8303–10

[68] Baig N, Kawde A N and Ibrahim M 2020 Efficient ionic medium supported reduced graphene oxide-based sensor for selective sensing of dopamine *Mater. Adv.* **1** 783–93

[69] Li T, Shen J, Chen G, Guo S and Xie G 2020 Performance Comparison of Proton Exchange Membrane Fuel Cells with Nafion and Aquivion Perfluorosulfonic Acids with Different Equivalent Weights as the Electrode Binders *ACS Omega* **5** 17628–36

[70] Lien N T, Quoc Hung L, Hoang N T, Thu V T, Ngoc Nga D T, Hai Yen P T, Phong P H and Thu Ha V T 2020 An Electrochemical Sensor Based on Gold Nanodendrite/Surfactant Modified Electrode for Bisphenol A Detection *J. Anal. Methods Chem.* **2020**

[71] Bacil R P, Chen L, Serrano S H P and Compton R G 2020 Dopamine oxidation at gold electrodes: Mechanism and kinetics near neutral pH *Phys. Chem. Chem. Phys.* **22** 607–14

[72] Kim Y-R, Bong S, Kang Y-J, Yang Y, Mahajan R K, Kim J S and Kim H 2010 Electrochemical detection of dopamine in the presence of ascorbic acid using graphene modified electrodes. *Biosens. Bioelectron.* **25** 2366–9

[73] Zhu W, Chen T, Ma X, Ma H and Chen S 2013 Highly sensitive and selective detection of dopamine based on hollow gold nanoparticles-graphene nanocomposite modified electrode *Colloids Surfaces B Biointerfaces* **111**

[74] Kwak M, Lee S, Kim D, Park S K and Piao Y 2016 Facile synthesis of Au-graphene nanocomposite for the selective determination of dopamine *J. Electroanal. Chem.* **776**

[75] Zhao L, Niu G, Gao F, Lu K, Sun Z, Li H, Stenzel M, Liu C and Jiang Y 2021 Gold Nanorods (AuNRs) and Zeolitic Imidazolate Framework-8 (ZIF-8) Core-Shell Nanostructure-Based Electrochemical Sensor for Detecting Neurotransmitters *ACS Omega* **6** 33149–58